Kondo-Majorana coupling in Double Quantum Dots.

by

Jesús David Cifuentes Pardo

Advisor: Luis Gregorio Dias da Silva

MASTER OF SCIENCE

in

Instituto de Física

(Condensed Matter Physics)

UNIVERSIDADE DE SÃO PAULO

(R. do Matão, 1371 - Butantã, São Paulo)

February 6, 2019

Chapter 1

Abstract

In the last decades the interest in the “search of Majorana fermions” in condensed matter systems [1] has increased due to their potential applications in quantum computing. As recently as 2012, experimental works reporting the detection of such quasiparticles [2, 3]. Later works [4, 5, 6, 7], including a recent paper published by the advisor of this dissertation and collaborators [8], set out to explore the interplay of such Majorana zero-modes with strongly interacting systems such as semiconductor quantum dots, which can be readily integrated in the device. This research project aims to expand this idea using the numerical renormalization group to study the model of a double quantum dot coupled to metallic leads and to a topological superconductor supporting edge Majorana zero modes. This simple model allows the manipulation of the majorana modes bringing possible applications to braiding procedures . In addition, we will study the interplay of Kondo correlations, exchange interactions and Majorana physics.

Chapter 2

Table of Contents

Chapter 3

Theory and Methods

In this chapter we describe the two methods that we will use to compute the density of states in this project. Using the ballistic transport method, we will obtain an exact analytical expression of this quantity for non-interacting systems (section 3.1). The physics of interacting systems is more complex and does not support an exact approach. Instead, we appeal to the renown numerical renormalization group (NRG) to deal with the strong correlations of these systems section 3.2 . Both models will be tested on the model of a double quantum dot attached to a metallic lead. We will observe that at very low energies, the physics of interacting systems emulates characteristic features of non-interacting models.

3.1 Ballistic transport

The Green function G of a Hamiltonian H is the operator that satisfies the homogeneous equation

$$\left(i\hbar\frac{\partial}{\partial t} - H\right) G\left(t-t'\right) = \delta(t-t'). \tag{3.1}$$

This type of differential equations are solved taking the Fourier transform

$$G_H(\omega) = \int_{-\infty}^{\infty} G(t-t')e^{i\omega(t-t')/\hbar}\delta(t-t') \tag{3.2}$$

In this new space the solution of the equation is

$$(\omega + is - H)G_\omega(\omega) = I.$$

The term $+is$ in the previous Hamiltonian is part of a mathematical trick quite common in this theory. During the whole procedure, the Green function acts on the complex field. But when we need to obtain a physical interpretation we will take the limit $s \to 0$ to obtain the result for real energies.

The next step is to decompose $G_H(\omega)$ in the eigenbase of the Hamiltonian $\{|\alpha\rangle\}$ by

$$\langle\alpha|G_H(\omega)|\alpha'\rangle = \frac{\delta_{\alpha\alpha'}}{\omega - is - \varepsilon_\alpha} = \frac{\delta_{\alpha\alpha'}(\omega + is - \varepsilon_\alpha)}{(\omega-\varepsilon_\alpha)^2 + s^2}. \tag{3.3}$$

From the famous formula

$$\lim_{s\to 0}\frac{s}{(\omega-\varepsilon_\alpha)^2+s^2} = \pi\delta(\omega-\varepsilon_\alpha) \tag{3.4}$$

we obtain

$$Im\langle\alpha|G_H(\omega)|\alpha'\rangle] = \pi\delta(\omega-\varepsilon_\alpha)\delta_{\alpha,\alpha'}. \tag{3.5}$$

Note that the sum of $Im[\langle\alpha|G_H(\omega)|\alpha'\rangle]$ over all the eigenstates of H is simply π times the density of states:

$$\rho(\omega) = -\frac{1}{\pi}\sum_\alpha Im\left[\langle\alpha|G_H(\omega)|\alpha'\rangle\right] = \sum_\alpha \delta(\omega-\varepsilon_\alpha). \tag{3.6}$$

An extended definition of the Green function can be given in terms of fermion operators in second quantization. The time-green function for two fermion operators A and B is

$$G_{A,B}(t-t') = \mathbb{T}[\{A(t),B(t')\}]. \tag{3.7}$$

In these problems, causality is important, which is the reason why we use the time-order operator $\mathbb{T}$. In addition, the evolution of this Green function is determined by Schroedinger's differential equation.

$$\frac{d}{dt}G_{A,B}\left(t-t'\right) = \langle\left[A(t),B(t')\right]\rangle\delta_{t-t'} + \langle\left[A(t),H'\right],B(t')\rangle \tag{3.8}$$

Once again, we perform a Fourier transform of $G_{A,B}(t-t')$ to obtain $G_{A,B}(\omega)$. When applying this transform to 3.8 we obtain

$$\omega G_{A,B}(\omega) = \delta_{A^\dagger,B} + G_{[A,H],B}(\omega). \tag{3.9}$$

Applying 3.9 to a set of operators $\{A_1,A_2,\ldots\}$ we obtain a whole set of transport equations describing the flow of state transitions of the operators in our model. In this thesis we will identify each set of equations with a flow graph. This will be our leading method to compute the green functions of the system.

Moreover, following equation 3.6 we can define the density of states associated to an operator A as

$$\rho_{A,A^\dagger} = -\frac{1}{\pi}Im\left[G_{A,A^\dagger}(\omega)\right]. \tag{3.10}$$

The density of states contains important physical information related to operator A. In our case, operator $A^\dagger$ will be related to the dot's creation operator $d^\dagger$. Hence computing 3.10 will allow us to observe the hybridization of the dot's discrete states and the creation of other energy levels due to the interaction with the lead and other possible impurities. We will observe examples of these computations in the following sections.

3.1.1 Using graph theory to solve the transport equations

Solving the transport equations involves dealing with a set of linear equations where all the possible variables including ω , and the Hamiltonian parameters are assumed to be constant. This can be done by Gauss-Jordan elimination, noting that after each elimination process we need to carry on the account in terms of the initial variables. The solution will be a polynomial fraction. When the number of operators in the Hamiltonian increases the number of terms in the polynomial grows-up rapidly according to the number of initial parameters. This reveals the importance of exploring new methods that could simplify the solution of this system, and present a readable factorized expression of the final solution.

The method presented here uses graph theory algorithms that provide a shortcut to Gauss-Jordan elimination [9]. To probe this method we solve here the transport equations for a non-interacting ($U = 0$) DQD connected to one lead.

According to the Anderson model the Hamiltonian for this system looks like

$$H = t_{dots} d_1^\dagger d_2 + t_{dots}^* d_2^\dagger d_1 + \sum_{i=1}^{2} \varepsilon_{di} d_i^\dagger d_i + \sum_k \left(V_i d_i^\dagger c_{\mathbf{k}} + V_i^* c_{\mathbf{k}}^\dagger d_i \right) + \varepsilon_{\mathbf{k}} c_{\mathbf{k}}^\dagger c_{\mathbf{k}}. \tag{3.11}$$

Since the system is non-interacting, we ignore the spin-degeneracy of this Hamiltonian. The only new parameter here is the term t_{dots}, which represents the tunneling between both quantum dots. Using equation (3.9) with $B = d_1^\dagger$ and A shifting among other operators we compute the following transport equations

$$(\omega - \varepsilon_1) G_{d_1, d_1^\dagger}(\omega) = 1 + t_{dots} G_{d_2, d_1^\dagger}(\omega) + V_1^* \sum_{\mathbf{k}} G_{c_{\mathbf{k}}, d_1^\dagger}(\omega) \tag{3.12}$$

$$(\omega - \varepsilon_{\mathbf{k}}) G_{c_{\mathbf{k}}, d_1^\dagger}(\omega) = V_1 G_{d_1, d_1^\dagger}(\omega) + V_2 G_{d_2, d_1^\dagger}(\omega) \tag{3.13}$$

$$(\omega - \varepsilon_2) G_{d_2, d_1^\dagger}(\omega) = t_{dots} G_{d_1, d_1^\dagger}(\omega) + V_2^* \sum_{\mathbf{k}} G_{c_{\mathbf{k}}, d_1^\dagger}(\omega) \tag{3.14}$$

This system is already closed which means that we don't need any other equation to find the solution. The associated matrix form is

$$\begin{bmatrix} \omega - \varepsilon_2 & -V_2 & -t_{dots} \\ -V_2^* & \omega - \varepsilon_k & -V_1 \\ -t_{dots}^* & -V_1^* & \omega - \varepsilon_1 \end{bmatrix} \begin{bmatrix} G_{c_{\mathbf{k}}, d_1^\dagger}(\omega) \\ G_{d_2, d_1^\dagger}(\omega) \\ G_{d_1, d_1^\dagger}(\omega) \end{bmatrix} = \begin{bmatrix} 0 \\ 0 \\ 1 \end{bmatrix} \tag{3.15}$$

By convenience we changed the order of the rows in the matrix and we removed the sum over k ($\sum_k$) to simplify the algebraic operation. We will insert these terms back in the equations at the end of the procedure.

Although this matrix is not Laplacian, the procedure in [9] can still be applied with the downside of loosing part of the speed-up of the algorithm. We still preserve some of the advantages using graphs, such as the possibility of taking minimal cuttings and the relation between

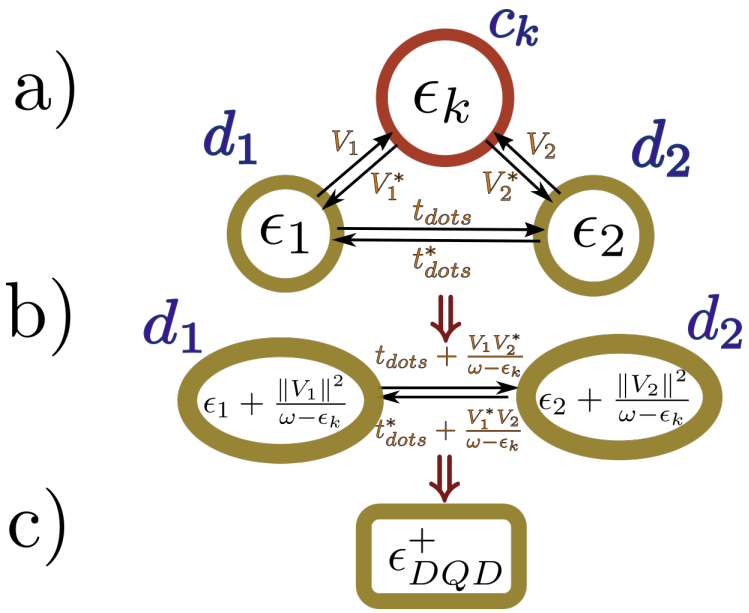

Figure 3.1: Graph representation of Gauss-Jordan elimination a) Graph $\mathscr{G}_{d_1 d_2}$ b) After the elimination of vertex c_k, the energies of dots d_1 and d_2, and the coupling parameter are changed. c) After Gaussian elimination of dot 2 the energy of the remaining dot $\varepsilon_D QD^+$ represents the transport information through d_1 of the entire DQD.

Source: *By the author.*

Gauss-Jordan elimination and random walks [9] . Both advantages simplify the complexity of the solution.

Now, our objective is to compute the green function $G_{d_{1\downarrow}, d_{1\downarrow}^\dagger}(\omega)$. For this we take the graph $\mathscr{G}_{d_1 d_2}$ associated to the matrix (3.15). See Figure 3.1.a). The vertexes of this graph are the operators in the first site of the of the green functions $(d_{1\downarrow}, d_2, c_k.\ d_1^\dagger)$. $d_1^\dagger$ is not included since it only appears in the second sub-index of the green functions. The edges are given by the non-diagonal sites in the matrix. In addition, an energy parameter is assigned to each vertex, according to the corresponding term in the diagonal. These energies can also be thought as the magnitude of edges connecting each vertex with itself. The plot of the energy parameters in this algorithm is quite important, hence we prefer to keep this name to differentiate them from the other couplings.

The algorithm consists in the following. Each step of Gauss-Jordan elimination leads to a new graph with different energies and couplings. The elimination of a row and column is equivalent to pop the corresponding vertex in the graph. For instance, lets eliminate the first row and column of the matrix in (3.15). For it we just need to subtract the rank-1 matrix with

the same first row and first column

$$\begin{bmatrix} \omega-\varepsilon_k & -V_2 & -V_1 \\ -V_2^* & \omega-\varepsilon_2 & -t_{dots} \\ -V_1^* & -t_{dots}^* & \omega-\varepsilon_1 \end{bmatrix} - \begin{bmatrix} \omega-\varepsilon_k & -V_2 & -V_1 \\ -V_2^* & \frac{V_2^*V_2}{\omega-\varepsilon_k} & \frac{V_2^*V_1}{\omega-\varepsilon_k} \\ -V_1^* & \frac{V_2V_1^*}{\omega-\varepsilon_k} & \frac{V_1^*V_1}{\omega-\varepsilon_k} \end{bmatrix} \tag{3.16}$$

$$= \begin{bmatrix} 0 & 0 & 0 \\ 0 & \omega-\varepsilon_2-\frac{V_2^*V_2}{\omega-\varepsilon_k} & -t_{dots}-\frac{V_2^*V_1}{\omega-\varepsilon_k} \\ 0 & -t_{dots}^*-\frac{V_2V_1^*}{\omega-\varepsilon_k} & \omega-\varepsilon_1-\frac{V_1^*V_1}{\omega-\varepsilon_k} \end{bmatrix} \tag{3.17}$$

The graph associated to this matrix can be observed in Figure 3.1.b) where operator c_k has been popped out of the graph. It is possible to associate the correction to the the energies and couplings to the possible walks passing through the vertex c_k. For instance d_1's energy ε_1 receives an extra-term $\frac{V_1^*V_1}{\omega-\varepsilon_k}$ representing an additional walk from d_1 to d_1 passing through c_k. The same logic can be applied to the other terms coupling terms. The correction to t_dots is $\frac{V_1^*V_2}{\omega-\varepsilon_k}$ which corresponds to a path from d_1 to d_2 passing through the popped vertex c_k. Note that this term includes the multiplication both couplings with the vertex divided by the difference of ω with the energy of the vertex. This correspondence between the energy correction and eliminated paths through the graph makes the "popping" process an straightforward task.

We now proceed to pop vertex d_2 which leaves just a single vertex as shown in Figure 3.1.c). The energy of it can be readily computed with the previous path elimination idea which gives

$$\varepsilon_{DQD}^{+} = \varepsilon_1 + \sum_{\mathbf{k}} \frac{V_1V_1^*}{\omega-\varepsilon_{\mathbf{k}}} + \frac{\left\| t_{dots} + \sum_{\mathbf{k}} \frac{V_1V_2^*}{\omega-\varepsilon_{\mathbf{k}}} \right\|^2}{\omega-\varepsilon_2-\sum_{\mathbf{k}} \frac{V_2V_2^*}{\omega-\varepsilon_{\mathbf{k}}}}, \tag{3.18}$$

where we selectively included the $\sum_k$-terms in the places where k appeared.

As a result of Gauss-Jordan elimination the linear equation in 3.15 has evolved into the trivial form

$$\begin{bmatrix} 0 & 0 & 0 \\ 0 & 0 & 0 \\ 0 & 0 & \omega-\varepsilon_{DQD}^{+} \end{bmatrix} \begin{bmatrix} G_{c_{\mathbf{k}},d_1^\dagger}(\omega) \\ G_{d_2,d_1^\dagger}(\omega) \\ G_{d_1,d_1^\dagger}(\omega) \end{bmatrix} = \begin{bmatrix} 0 \\ 0 \\ 1 \end{bmatrix}. \tag{3.19}$$

The Green function is then

$$G_{d_1,d_1^\dagger}(\omega) = \frac{1}{\omega-\varepsilon_{DQD}^{+}} = \left[\left(\omega-\varepsilon_1-\sum_{\mathbf{k}} \frac{V_1V_1^*}{\omega-\varepsilon_{\mathbf{k}}} \right) - \frac{\left(t_{dots}+\sum_{\mathbf{k}} \frac{V_1V_2^*}{\omega-\varepsilon_{\mathbf{k}}} \right) \left(t_{dots}+\sum_{\mathbf{k}} \frac{V_1V_2^*}{\omega-\varepsilon_{\mathbf{k}}} \right)^*}{\omega-\varepsilon_2-\sum_{\mathbf{k}} \frac{V_2V_2^*}{\omega-\varepsilon_{\mathbf{k}}}} \right]^{-1}. \tag{3.20}$$

This Green function will be very important in the following chapters where we will compare its behavior with the green function of a Majorana mode.

3.1.2 Graph Algorithm

In this part we summarize the steps of the graph algorithm in order to apply them later to more complicated systems:

1. Computing the transport equations with the second term fixed in the creation operator of $d^\dagger$.
2. Writing the graph associated to the transport system. The vertexes are the operators in the first site of the of the green functions. Energies and couplings are associated to the vertex and edge numbers of the graphs respectively.
3. Popping the vertexes of the graph. Each vertex popping involves the following steps.
   (a) Computing the extra-terms in the energies and couplings based on the walks passing through the popped vertex.
   (b) Eliminating this vertex from the graph.
   (c) Iterating till there is only the vertex d.
4. The energy in the remaining vertex d is $\varepsilon_d = \frac{1}{\omega - G_{d,d^\dagger}(\omega)}$.

This algorithm will be our main method to find the green function and therefore the density of states of any interacting system.

3.1.3 Ballistic transport in a double quantum dot

In this subsection we describe the remaining steps to extract the density of states of the double quantum dot from the Green function 3.20. We will plot the results and observe the evolution of the DOS while tuning the parameters of the model.

First note that equation (3.20) depends on the term $\sum_k \frac{V_i^* V_j}{\omega - \varepsilon_k}$ which describes the broadening of the DOS when the QD enters in contact with the lead. This broadening is usually named $\Gamma_i = V_i^* V_i$ (Or Δ depending on the text book). In general V_i is a function of $\mathbf{k}$. However, in the limit of flat-band we can assume that V_i is constant. Therefore, it is enough to integrate

$$\sum_k \frac{1}{\omega - \varepsilon_k + is} = \int_{-D}^{D} \frac{d\varepsilon_k}{\omega - \varepsilon_k + is} = -\ln\left(\frac{D - \varepsilon_k + is}{-D - \varepsilon_k + is}\right) \xrightarrow[D\to\infty]{} -i, \tag{3.21}$$

where we assumed that there is a maximum energy cutoff D going to infinity in the wide-band limit. Hence

$$-i\Gamma_i = \sum_k \frac{V_i^* V_i}{\omega - \varepsilon_k}. \tag{3.22}$$

We can replace this in equation (3.20) to obtain the real expression for the green function $G_{d_1,d_1^\dagger}(\omega)$. The terms of the form $V_1 V_2^*$ can be replaced for $\sqrt{\Gamma_1 \Gamma_2}$, supposing there is no additional complex phase.

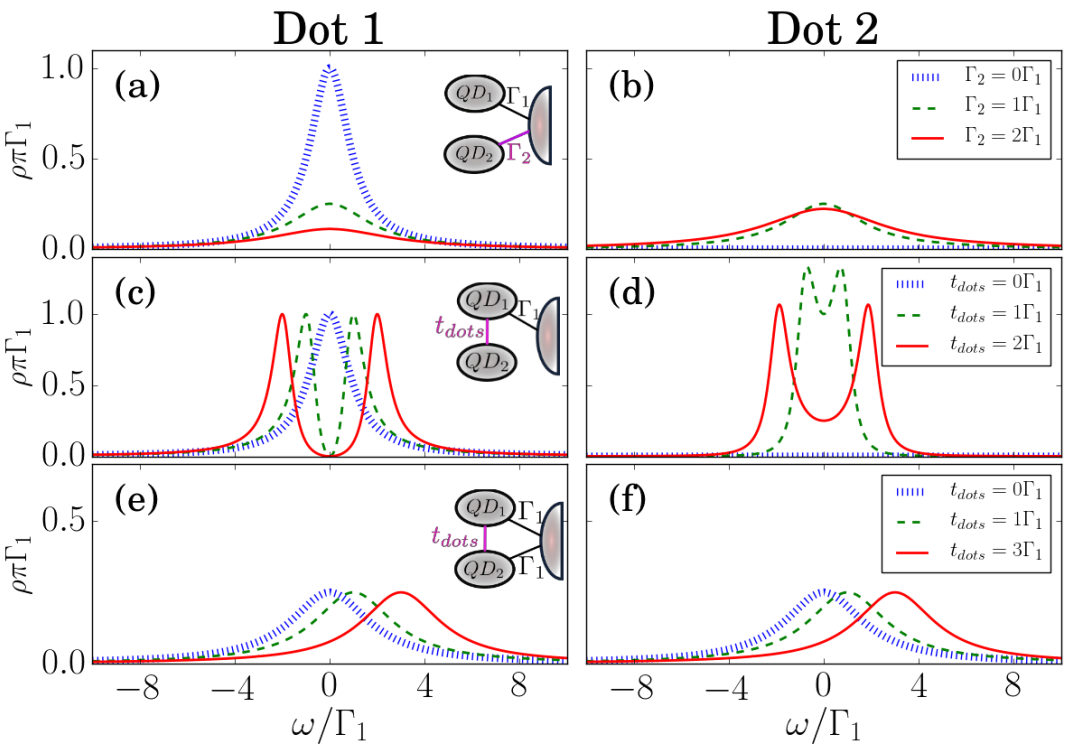

Figure 3.2: Evolution of the density of states at each QD (Left: dot 1, Right: dot 2) at three distinct arrangements of DQD-lead coupling. The inset at the first column depicts the type of coupling. The purple line represents the tuning variable. The energy unit is Γ_1. $e_1 = e_2 = 0$ in all arrangements. (a),(b) The lead is connected to both QDs. Tuning variable: Γ_2. (c)(d) Indirect coupling of the second dot through dot one. Tuning variable: $\_dots$. (e)(f) Triangular coupling. Tuning variable: t_{dots}.

Source: *By the Author*

Now, remember from (3.10) that the DOS ρ depends on the imaginary factor of the Green Function $G_{d_1,d_1^\dagger}(\omega)$. This term depends in the broadening Γ. If $\Gamma = 0$ the density of states will be 0 as well. At any other case, one of the dots should be attached to the lead. Let Γ_1 be the broadening of this dot. We will take Γ_1 as our natural unit for the rest of this thesis.

In Figure 3.2 we can observe the evolution of the Density of States under certain processes. Each plot includes an inset showing the model applied to the figure. The coupling in purple indicates the tuning variable. We set $e_1 = e_2 = 0$ so that both dots satisfy PHS. The primary results are the

1. **Coupling QD2. Figure 3.2(a)(b):** At $\Gamma_2 = 0$ the second dot is decoupled, hence the first dot's DOS is the same of a single dot case. The maximum height is achieved at $\rho\pi\Gamma_1 = 1$

and the width of this peak is about Γ_1, just as in Figure **??**. When the second dot is attached $\Gamma_2 > 0$ the density of states is divided between both dots. At $\Gamma_1 = \Gamma_2$ the DOS at the Fermi energy is equal to $\frac{1}{4\pi\Gamma}$ for both dots. For higher values of Γ_2 the DOS in the second dot is higher than in the first one.

2. **Indirect Coupling of QD2. Figure 3.2(c)(d):** This is case is interesting. When the second dot is connected indirectly through the first dot, quantum inference splits the central peak in two new states. We will observe later that in the interacting case this procedure can also destroy the Kondo signature. Note that the higher the coupling t_{dots} is, the greater is the gap between the states. We will usually take $t_{dots} = 2\Gamma_1$ to make these gap more visible in the NRG simulations.

3. **Breaking Particle Hole Symmetry. Figure 3.2(e)(f):** Suppose we have $\Gamma_2 = \Gamma_1$. The "triangular connections" break Particle Hole Symmetry. The central peak is displaced to the positive part of the spectrum. We will avoid this situation during this project, because because PHS-breaking will prevent the Majorana to tunnel inside the DQD. Hence, this model won't lead to any interesting result on Majorana manipulation.

3.2 The Numerical Renormalization Group (NRG)

3.2.1 From the Renormalization Group to the Wilson's Chain

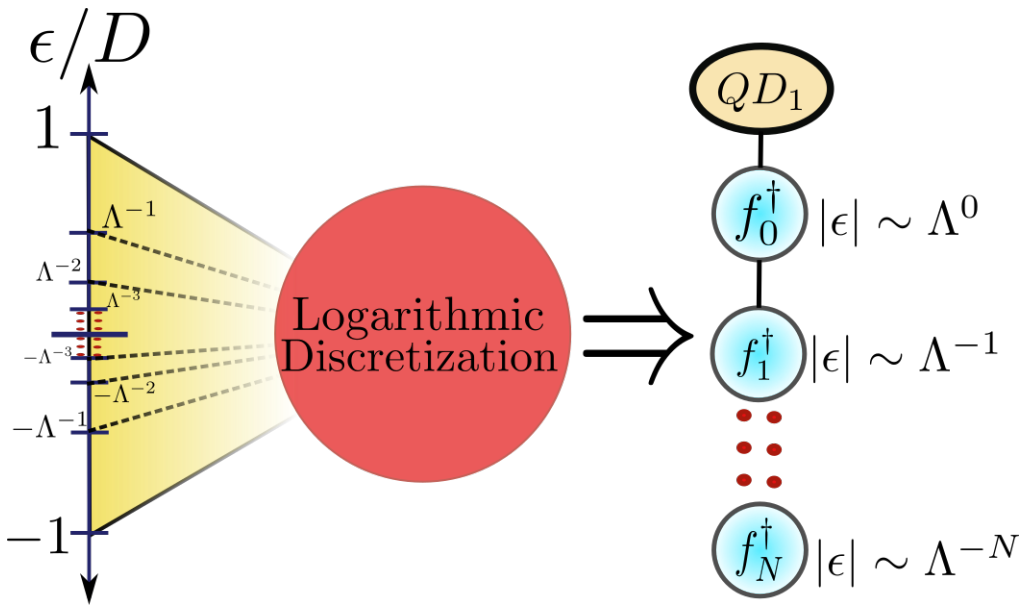

Figure 3.3: . Energy interval discretization. Source: *By the Author*

The real meaning of divergent logarithmic term in the resistivity predicted by Kondo is that important contributions at low-energy scales caused by the strong quantum correlations in the system are being neglected by perturbation theory. This problem can be solved by introducing ideas from renormalization group theory. A renormalization approach is more adequate for this type of problem since it assigns an appropriate effective Hamiltonian to each scale of temperature. This provides a more accurate representation of the increasing density of correlated states appearing close the Fermi energy.

In renormalization group theory, the Hamiltonian transformations are performed by an operator $\mathscr{T}$ that represents an endomorphism in the space of operators. T generates the semigroup $\{1, \mathscr{T}, \mathscr{T}^2, \ldots\}$, that defines a complete set of transformations

$$\mathscr{T}[H_0] = H_1,\ \mathscr{T}[H_1] = H_2, \ldots, \mathscr{T}[H_N] = H_{N+1}, \ldots$$

If $\mathscr{T}$ is a contracting map [1] then it is known that this set of operations should eventually lead to a fix point $\mathscr{T}^N[H] \xrightarrow{N\to\infty} H*$ such that $\mathscr{T}[H*] = H*$. In numerical simulations, N will only increase up to a value where H_N is close enough to the fix point $H*$ so that no new significant contributions to the Hamiltonian are obtained. For the purposes of this project, taking $N = 51$ will be enough for the NRG code to converge.

In the 1970's G.Wilson used this theory to create the famous Numerical Renormalization Group (NRG) [10, 11, 12]. His main idea was to perform a logarithmic discretization of the conduction band in the lead as shown in Figure 3.3.(a). Taking into account that the leading contributions to the conductance occur at states close to the Fermi energy $\omega = 0$, we can define a cut-off ($|\omega| < D$) so that the rest at higher contributions are not relevant.Then we use D to rescale the energy interval. As you can observe in the figure, the QD is coupled to all these energy states at the same time. The logarithmic discretization gives more relevance to the low energy scales by assigning a different Hamiltonian coupling to each one of them. To complete this idea, the NRG code maps the Hamiltonian of the QD-lead system to the Wilson's chain shown in Figure 3.3(b). A detailed description of this map is included in the Appendix section A.1.

After these steps we obtain a chain Hamiltonian of the form

$$H = H_d + D\sum_{\sigma}\left[\sqrt{\frac{2\Gamma}{\pi D}}\left(d_\sigma^\dagger f_{0\sigma} + f_{0\sigma}^\dagger d_\sigma\right) + \frac{1}{2}\left(1+\Lambda^{-1}\right)\sum_{n=0}^{\infty}\Lambda^{\frac{-n}{2}}\xi_n\left(f_{n\sigma}^\dagger f_{n+1,\sigma} + f_{n+1\sigma}^\dagger f_{n\sigma}\right)\right]. \tag{3.23}$$

In the flat-band approximation the parameters ξ_n can be obtained analytically [10]

$$\xi_n = \frac{1-\Lambda^{-n-1}}{\left(1-\Lambda^{-2n-1}\right)^{\frac{1}{2}}\left(1-\Lambda^{-2n-3}\right)^{\frac{1}{2}}}.$$

From equation (A.12) we define the following set of Hamiltonians

[1] Let $\mathscr{O}$ be a set of operators, then T is a contracting map if $\mathscr{T}[\mathscr{O}'] \subset \mathscr{O}'$ for every $\mathscr{O}' \subset \mathscr{O}$.

$$H_{N+1} = T\left[H_N\right] = \Lambda^{-\frac{1}{2}} H_N + \xi_N \left(f^{\dagger}_{N+1,\sigma} f_{N,\sigma} + f^{\dagger}_{N,\sigma} f_{N+1,\sigma} \right), \tag{3.24}$$

with

$$H_{-1} := \frac{2H_d}{1+\Lambda^{-1}}. \tag{3.25}$$

The Renormalization Group transformation $\mathscr{T}$ can be defined as

$$\mathscr{T}^N H_{-1} = \frac{1+\Lambda^{-1}}{2} \Lambda^{\frac{N-1}{2}} H_N$$

Note that in the limit $\xrightarrow{N\to\infty}$ we should recover the initial Anderson Hamiltonian. In addition, note that the leading coefficients of the contributions to each Hamiltonian H_N are given by

$$\Lambda^{\frac{-N}{2}} \xi_N \xrightarrow{N\to\infty} \frac{\Lambda^{\frac{-N}{2}} \left(1-\Lambda^{-N}\right)}{1-\Lambda^{-2N}} \sim \frac{\Lambda^{\frac{-N}{2}}}{1+\Lambda^{-N}},$$

which decays exponentially with the length of the chain. Therefore, we may thing that at some point these new contributions will be so small that the that the map $\mathscr{T}$ will eventually converge. Formally the theory regarding the NRG convergence is to complex for this thesis. However the results show that the operator that trully converges is $\mathscr{T}^2$ and not $\mathscr{T}$[12]. This has important consequences, for instance the convergence of the code has to be analyzed on odd and even values of N separately.

To this point the expression (A.12) and the derived limit of H_N to the Anderson Hamiltonian are exact. The first approximations arrive in the following step which include an iterative diagonalization of the Hamiltonian.

3.2.2 Iterative Diagonalization

This diagonalization starts with the impurity/dot Hamiltonian H_{-1}, which must be written in matrix form according to a defined basis. The other steps can be defined by induction. Suppose that the spectrum of H_N is diagonal on a given basis. Then the NRG code performs each of the following steps:

1. Rescaling the spectrum of H_N by $\Lambda^{\frac{1}{2}}$ as defined in A.12. Figure 3.4 (a)→(b).

2. Adding the next step of the chain to form H_{N+1} and diagonalizing the new Hamiltonian such that $H_{N+1} = U^{\dagger}_{N+1} D_{N+1} U_{N+1}$. After this step, each of the eigenstates of H_N will spit in up to 4 new energy states (probably degenerate) determined by the new coupling with the $N+1$ site basis $|0\rangle, |\uparrow\rangle, |\downarrow\rangle, |\uparrow\downarrow\rangle$. Figure 3.4 (b)→(c).

3. Shifting the spectrum by a certain dephase factor such that the 0 of energy is always the ground state. Figure 3.4 (c)→(d).

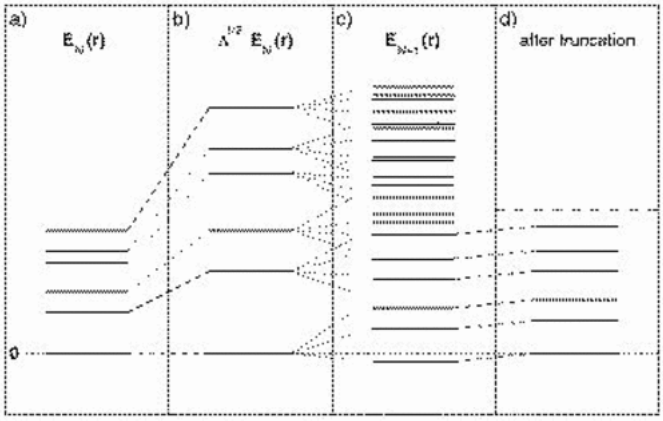

Figure 3.4: Iterative diagonalization process. Source: *By the Author*

4. Numerical cutting: If the number of states in the system exceeds a definite number (1000 in this thesis) the exceeding higher energy states are neglected.[2]. Figure 3.4 (c)→(d).

5. Rotating operators $f_{N,\sigma}$ by $U_N f_{N,\sigma} U_N^\dagger$ to start the next operation.

The final outcome of this operations will be the complete spectrum of the Anderson model at each energy level. However we still need to talk about an important speed-up to the code obtain when considering the symmetries of the system.

3.2.3 Symmetries

The symmetries of the initial Hamiltonian take a very important role in this iterative diagonalization. Lets suppose that the initial Hamiltonian H_d has certain symmetries classified by the quantum number S . Then H_d can be written can be represented in block Hamiltonians over a basis of the form $|S,i\rangle$. A diagnolization process of an square matrix with L rows usually has an square order proportionate to the number of entries $\mathcal{O} \sim L^2$. However, if the matrix is organize in blocks of length N_j such that $\sum_j L_j = L$, then the order of diagonalization will be around $\sum_j L_j^2$ which is in general much smaller than $(\sum_j L_j)^2 L^2$. Therefor the block diagonalization provides important numerical advantages to the algorithm.

To keep this speed-up we must preserve this symmetry structure for the rest of the algorithm. For it, we first need to verify that the picked symmetry also commutes with the hopping terms in the chain Hamiltonian. If so, for each step N of the NRG algorithm we will have that the H_N Hamiltonian can be written in a block diagonal form with basis $|S_N, i_N\rangle$. Then it is necessary to

[2]This step must be performed carefully to preserve the symmetries of the system. If two states are entangled and one of them is eliminated and the other is not, the program could lead to misleading results. Further discussions to solve this problem are presented in the symmetry subsection.

define transition rules from the quantum numbers S_N to S_{N+1}. By doing this, we assure that the block architecture is transmitted through the entire algorithm, hence reducing the computational time significantly at each step of the NRG chain.

In the following subsection we will give examples of this symmetry propagation in the example a quantum dot attached to a metallic lead.

3.2.4 Iterative Diagonalization in a Single QD Hamiltonian

Now that we have an iterative representation of the Anderson Model Hamiltonian (A.12), lets take a look to how the NRG code would work for a QD. We start with the dot Hamiltonian. (Since the D term is always present as a normalizing factor, we are going to avoid this term in future computations and suppose that we are working with unit-less variables ε_d, U and $\Gamma' := \sqrt{\frac{2\Gamma}{\pi D}}$).

$$H_d = \frac{1}{D}\left(\varepsilon_d + \frac{U}{2}\right) d^\dagger_\sigma d_\sigma + \frac{U}{2D}(d^\dagger_\sigma d_\sigma - 1)^2. \tag{3.26}$$

Now observe that hamiltonian 3.26 already has a diagonal form in the base $\{|\uparrow\downarrow\rangle, |\uparrow\rangle, |\downarrow\rangle, |0\rangle\}$

$$H_d = \frac{1}{D}\begin{bmatrix} 2\varepsilon_d + \frac{3U}{2} & 0 & 0 & 0 \\ 0 & \varepsilon_d + \frac{U}{2} & 0 & 0 \\ 0 & 0 & \varepsilon_d + \frac{U}{2} & 0 \\ 0 & 0 & 0 & \frac{U}{2} \end{bmatrix}.$$

Lets define $H_{-1} = \Lambda^{\frac{-1}{2}} H_d$. Adding the first chain interaction to H_d we obtain a new Hamiltonian of the form

$$H_0 = \Lambda^{\frac{1}{2}} H_{-1} + \Gamma'\left(d^\dagger_\sigma f_{0\sigma} + f^\dagger_{0\sigma} d_\sigma\right). \tag{3.27}$$

The Hilbert space for this Hamiltonian has to be extended to include the 4 degrees of freedom of the $f^\dagger_{0\sigma}$ particles which are also given by $\{|\uparrow\downarrow\rangle, |\uparrow\rangle, |\downarrow\rangle, |0\rangle\}$. Therefore the total Hilbert space for H_0 is given by a base of the form

$$|s_1\rangle|s_2\rangle := |s_1\rangle \otimes |s_2\rangle \text{ with } |s_i\rangle \in \{|\uparrow\downarrow\rangle, |\uparrow\rangle, |\downarrow\rangle, |0\rangle\}.$$

We obtain an space of dimension $4 \times 4 = 16$. Now, before adventuring to write the Hamiltonian for H_0 as a 16×16-matrix note that H_{-1} preserves particle number $\mathscr{N}$ and the total spin S. We can associate each state to one of these symmetries as

$$|\uparrow\downarrow\rangle \longrightarrow |\mathscr{N} = 2, S = 0\rangle \text{ , } |0\rangle \longrightarrow |\mathscr{N} = 0, S = 0\rangle \tag{3.28}$$

$$|\uparrow\rangle \longrightarrow |\mathscr{N} = 1, S = \frac{1}{2}\rangle \text{ , } |0\rangle \longrightarrow |\mathscr{N} = 1, S = \frac{-1}{2}\rangle. \tag{3.29}$$

The propagation rule for the symmetry is defined with the following identity

$$|\mathscr{N}_1, S_1\rangle \otimes |\mathscr{N}_2, S_2\rangle \subset |\mathscr{N}_1 + \mathscr{N}_2, S_1 + S_2\rangle \tag{3.30}$$

Then we can use $\mathscr{N}$ and S as quantum numbers and generate the Hamiltonian H_0 in blocks. We will observe that the terms in the diagonal will correspond to the eigenvalues of H_{-1} for the first space. The non-diagonal terms are the result of the hopping interactions with the first site.

$H_{\mathscr{N}=0,S=0}$:

$$|0\rangle|0\rangle \rightarrow \quad \left[\tfrac{U}{2}\right]$$

$H_{\mathscr{N}=4,S=0}$:

$$|\uparrow\downarrow\rangle|\uparrow\downarrow\rangle \rightarrow \quad \left[2\varepsilon_d + \tfrac{3U}{2}\right]$$

$H_{\mathscr{N}=1,S=\frac{1}{2}}$:

$$\begin{array}{c} |\uparrow\rangle|0\rangle \rightarrow \\ |0\rangle|\uparrow\rangle \rightarrow \end{array} \begin{bmatrix} \varepsilon_d + \frac{U}{2} & \Gamma' \\ \Gamma' & \frac{U}{2} \end{bmatrix}$$

$H_{\mathscr{N}=1,S=\frac{-1}{2}}$:

$$\begin{array}{c} |\uparrow\rangle|0\rangle \rightarrow \\ |0\rangle|\uparrow\rangle \rightarrow \end{array} \begin{bmatrix} \varepsilon_d + \frac{U}{2} & \Gamma' \\ \Gamma' & \frac{U}{2} \end{bmatrix}$$

$H_{\mathscr{N}=2,S=-1}$:

$$|\downarrow\rangle|\downarrow\rangle \rightarrow \quad \left[\varepsilon_d + \tfrac{U}{2}\right]$$

$H_{\mathscr{N}=2,S=1}$:

$$|\uparrow\rangle|\uparrow\rangle \rightarrow \quad \left[\varepsilon_d + \tfrac{U}{2}\right]$$

$H_{\mathscr{N}=2,S=0}$:

$$\begin{array}{c} |\uparrow\downarrow\rangle|0\rangle \rightarrow \\ |\uparrow\rangle|\downarrow\rangle \rightarrow \\ |\downarrow\rangle|\uparrow\rangle \rightarrow \\ |0\rangle|\uparrow\downarrow\rangle \rightarrow \end{array} \begin{bmatrix} 2\varepsilon_d + \frac{3U}{2} & \Gamma & -\Gamma & 0 \\ \Gamma & \varepsilon_d + \frac{U}{2} & 0 & \Gamma \\ -\Gamma & 0 & \varepsilon_d + \frac{U}{2} & -\Gamma \\ 0 & \Gamma & -\Gamma & \frac{U}{2} \end{bmatrix}$$

$H_{\mathscr{N}=3,S=\frac{1}{2}}$:

$$\begin{array}{c} |\uparrow\downarrow\rangle|\uparrow\rangle \rightarrow \\ |\uparrow\rangle|\uparrow\downarrow\rangle \rightarrow \end{array} \begin{bmatrix} \varepsilon_d + \frac{U}{2} & -\Gamma' \\ -\Gamma' & \frac{U}{2} \end{bmatrix}$$

$H_{\mathscr{N}=3,S=\frac{-1}{2}}$:

$$\begin{array}{c} |\uparrow\downarrow\rangle|\downarrow\rangle \rightarrow \\ |\downarrow\rangle|\uparrow\downarrow\rangle \rightarrow \end{array} \begin{bmatrix} \varepsilon_d + \frac{U}{2} & -\Gamma' \\ -\Gamma' & \frac{U}{2} \end{bmatrix}$$

The next step would be to diagonalize H_0 by blocks $H_{\mathscr{N},S}$ and then including the next place in the chain. The following Hamiltonians are generated in the same way from equation 3.24. The symmetries of the new states can be obtained from the propagation rule 3.30. When the number of states surpasses the 1000 states, the code will automatically cutoff the higher energy states. However it is important that a Block is not divided in this cutting, since it could break the preserved symmetry.

Finally, the spectrum for $\Lambda = 2.5$ takes the 'spaghetti' form in Figure 3.5. Before $N = 30$ low-energy contributions generate significant changes in the energy levels. The stable strum after the step $N = 30$ shows that the code has converged at this stage. As we previously declared, it is not $\mathscr{T}$ but $\mathscr{T}^2$ the transformation that has fixed points, which explains why it was necessary to plot the even and the odd spectrum separately.

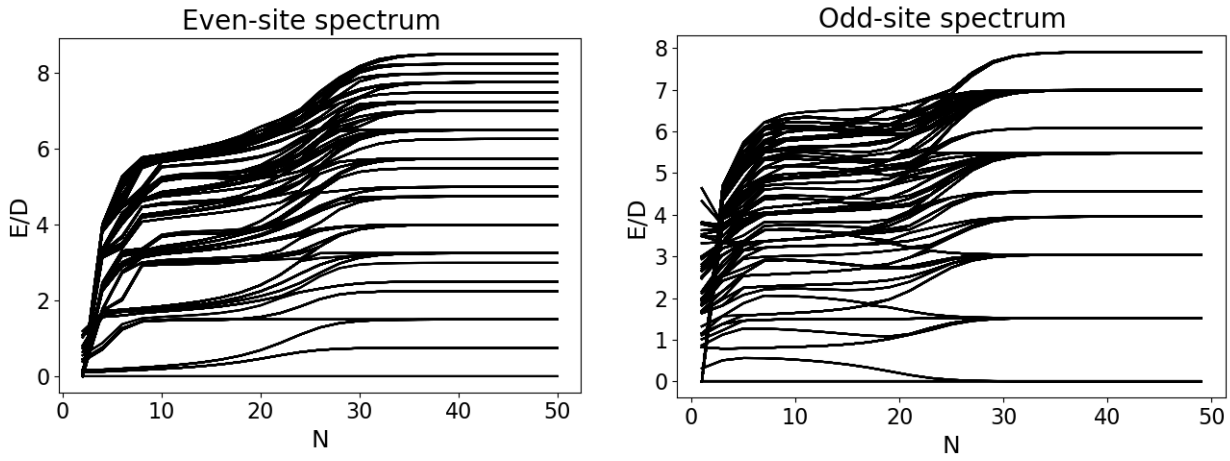

(a) N takes only even values

(b) N run only through odd values

Figure 3.5: Evolution of the QD-spectrum vs number of iterations of the code for $U = 0.5$, $e_d = -0.25$, $\Gamma = 2.82 \times 10^{-2}$.

At the end of the NRG code, we obtain a complete list of the spectrum $(E_{i,N})$ and the eigenstates $(|i,N\rangle)$ of the Hamiltonian at each step N of the chain (See Figure 3.5). It is important to keep all of these states since each one of them represents different thermodynamic regimes of the system. While the site $N = 1$ represents the physics of the system relevant at temperatures around $K_B D\Lambda^{-1}$, the site $N = 30$ shows the low energy contributions at $T \sim K_B D\Lambda^{-30}$ where the ground state is strongly correlated. Furthermore, the states at low temperatures are entangled with the higher energy states. We need to take this into account to extract dynamical quantities of the system, which is the objective of the following section.

3.2.5 The Density Matrix Renormalization Group (DM-NRG)

The NRG codes allows us to compute several thermodynamic quantities such as the entropy S, the free energy and the partition function $Z(\beta)$. In addition, we can compute the spin magnetization or dynamical quantities such the density of states, the magnetic susceptibility and the conductivity. To perform this we can use the spectrum obtained in the NRG code to define the Boltzman distribution of the system. Then we apply the usual methods of statistical mechanics.

In this thesis we will focus in computing the density of states at the impurity (QD). For this, let $|j\rangle$ and $|q\rangle$ label a base of eigenstates of the Hamiltonian H. Now recall the definition of the time-ordered green function 3.7

$$G_{d,d^\dagger}(t) = \left\langle \mathbb{T}\left[d(t)d^\dagger(0)\right]\right\rangle \tag{3.31}$$

$$= \theta(t)\left\langle \left[e^{\frac{i}{\hbar}Ht}de^{-\frac{i}{\hbar}Ht}d^\dagger\right]\right\rangle + \theta(-t)\left\langle \left[d^\dagger e^{\frac{i}{\hbar}Ht}de^{\frac{-i}{\hbar}Ht}\right]\right\rangle \tag{3.32}$$

$$= \theta(t)\sum_{|j\rangle,|q\rangle} p_j\langle j|e^{\frac{i}{\hbar}Ht}d|q\rangle\langle q|e^{-\frac{i}{\hbar}Ht}d^\dagger|j\rangle + \theta(-t)\sum_{|j\rangle,|q\rangle} p_q\langle q|d^\dagger e^{\frac{i}{\hbar}Ht}|j\rangle\langle j|de^{-\frac{i}{\hbar}Ht}|q\rangle \tag{3.33}$$

$$= \theta(t)\sum_{|j\rangle,|q\rangle} p_j e^{\frac{-i}{\hbar}t\left(E_j-E_q\right)}\left\|\langle j|d|q\rangle\right\|^2 + \theta(-t)\sum_{|j\rangle,|q\rangle} p_q e^{\frac{i}{\hbar}t\left(E_j-E_q\right)}\left\|\langle j|d|q\rangle\right\|^2 \tag{3.34}$$

Where $p_j := \frac{e^{-\beta E_j}}{Z(\beta)}$ defines the Boltzmann probability of the eigenstate $|j\rangle$ according to Hamiltonian H.

It is known that the Fourier transform of an expression of the form $e^{-ax}\theta(x)$ is $\frac{1}{\omega+is-a}$. Then the Green function in the frequency space is

$$G_{d,d^\dagger}(\omega) = \frac{1}{Z(\beta)}\sum_{|j\rangle,|q\rangle}\frac{e^{-\beta E_j}+e^{-\beta E_q}}{\omega+is-E_j+E_q}\left\|\langle j|d|q\rangle\right\|^2. \tag{3.35}$$

From the imaginary part of 3.35 we obtain a formula for the spectral density in terms of the eigenstates and energies of the Hamiltonian

$$\rho_d = \frac{1}{Z(\beta)}\sum_{|j\rangle,|q\rangle}\left(e^{-\beta E_j}+e^{-\beta E_q}\right)\delta\left(\omega-E_j+E_q\right)\left\|\langle j|d|q\rangle\right\|^2. \tag{3.36}$$

This new expression for the DOS can be integrated to NRG code in different ways . A first method created by Costi *et al.* consisted in computing (3.36) with the eigenstates of each shell Hamiltonian H_N [13]. It is necessary to take into account that the operator $\langle j|d|q\rangle$ is constantly rotating after each diagonalization procedure generating different representation. Then, an important part of Costi's algorithm is to obtain these new representations of $\langle j|d|q\rangle_N$ recursively starting from an input representation $\langle j|d|q\rangle_{N=0}$.

Although Costi's method predicts accurately the DOS at low-energies, it fails to fit the high energy levels. The method that corrects this problem receives the name of Density Matrix Numerical Renormalization Group (DMNRG) [14]. The main idea of DMNRG is to include the entanglement corrections with the lower energy-states using the density matrix formalism. For this, Hofstetter defines the density matrix at the last shell Hamiltonian N_{max} $\hat{\rho}$ as the thermal mixed state

$$\hat{\rho}_{N_{max}} = \sum_j e^{-\beta E_j}|j\rangle_{Nmax}\langle j|, \tag{3.37}$$

where the subindex N_{max} pinpoints that $|j\rangle_{Nmax}\langle j|$ is an eigenstate of the last shell Hamiltonian H_{N_max}.

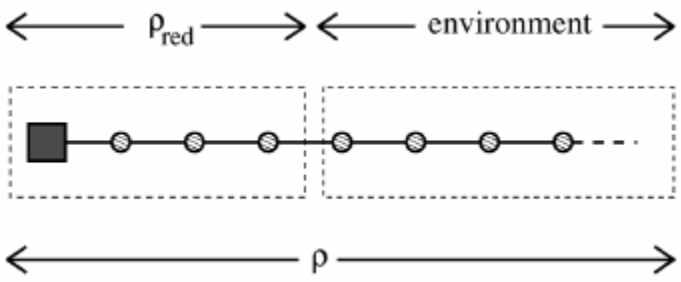

Figure 3.6: Wilson's chain depicted as an open quantum system.

With this new density matrix we could rewrite 3.32 as

$$G^{N_{max}}_{d,d^\dagger}(t) = \mathrm{Tr}\left(\hat{\rho}_{N_{max}} \mathbb{T}\left[\left\{d^\dagger, d\right\}\right]\right). \quad (3.38)$$

From the Green function $G^{N_{max}}_{d,d^\dagger}(t)$ we can obtain the density of states associated to the temperature T_{N_max}. Nevertheless, these results are not relevant at higher temperatures.

To solve this problem we may think Wilson's chain as an open quantum system where the reservoir are the low-energy sites of the chain and the system contains the high energy site including the impurity/QD as observed in Figure 3.6. Using this analogy it is possible we can readily obtain the density matrix ρ_S by taking the partial trace over the reservoir

$$\rho_s = \mathrm{Tr}_R[\rho_{N_{max}}]. \quad (3.39)$$

The DM-NRG code applies recursively this idea to obtain the density matrix corresponding to each scale of temperature T_N. It starts from $\rho_{N_{max}}$ defined at (3.37) and obtains $\rho_{N_{max}-1}$ by taking the partial trace over the vector space corresponding to the last site of the chain

$$\rho_{N_{max}-1} = \mathrm{Tr}_{N_{max}}[\rho_{N_{max}}]. \quad (3.40)$$

The other density matrices are computed by induction as

$$\rho_{N-1} = \mathrm{Tr}_N[\rho_N], \quad (3.41)$$

and the density of states at each temperature regime can be computed at each stage from the green function

$$G^{N}_{d,d^\dagger}(t) = \mathrm{Tr}\left(\hat{\rho}_N \mathbb{T}\left[\left\{d^\dagger, d\right\}\right]\right). \quad (3.42)$$

The DM-NRG algorithm produces significantly better results at high energies than Costi's initial idea. Indeed, DM-NRG is still one of the best methods to compute dynamic quantities of an impurity system. In the following subsection we will some details of how DM-NRG is integrated with the NRG code.

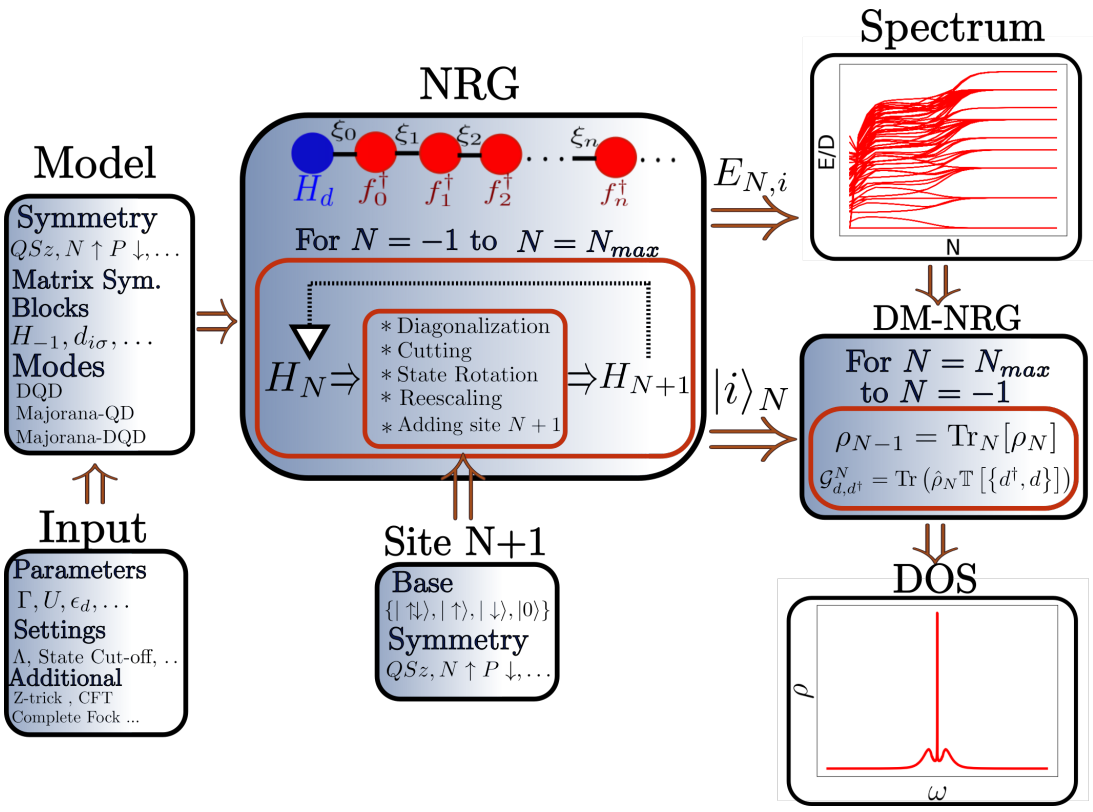

Figure 3.7: Diagram of the NRG code

3.2.6 Specifications of the NRG Code

The NRG code used in this thesis was implemented by my thesis advisor Luis Gregorio Dias during his posdoc at the University of Ohio. The general scheme is shown in Figure 3.7. It incorporates different stages in order to complete the procedure described in this classes. Here we give a brief description of each step:

- **Model:** The model defines the type of impurity that we are going to study. It could be a single QD or more complex structures such as a DQD or a Majorana-QD system. My main contribution to this code was at this stage by designing the mode DQD-Majorana, which describes a DQD coupled to a Majorana zero mode. These models preserve different symmetries. In the single dot Hamiltonian presented in subsection 3.2.4 we used the symmetry $\mathcal{N}S_z$, which is equivalent to charge-spin QS_z. However we will find that Majorana systems require another symmetry-type that we call as $N\uparrow P\downarrow$. The model is defined by initial Hamiltonian H_{-1} and the annihilation operators $d_{i\sigma}$ which must be submitted in the code written in the block symmetry representation described in subsection 3.2.3.

- **Input:** The input is a .dat file that attributes a numerical value to each parameter of the model. In addition, it allows to set different code specifications as the number of iterations N_{max}, the scaling parameter Λ and the maximum number of states before the cut-off. It is also possible to include additional implementations to improve the results of the NRG code such as the Z-trick [15] and the Complete Fock State. In this project, we only used the Z-trick, which significantly improves the spectral resolution at high energies.

- **NRG-Main:** This part of the code mainly integrates the ideas of subsection 3.2.1 and implements the iterative diagonalization described in subsection 3.2.2. Each shell Hamiltonian H_n is diagonalized. The high-energy eigenstates are cut-off if they exceed the limit. Then the states are rotated and the eigenvalues are rescaled to include the next step of the Wilson's chain. The symmetry block structure is preserved during the entire loop. NRG produces as out a detailed evolution of the spectrum which produces the spaghetti form. In addition, it can print the states and operators that are necessary to start other instances of the code like DM-NRG.

- **Site** $N+1$**:** This is an small class that creates another site of the chain in the base $\{|\uparrow\downarrow\rangle, |\uparrow\rangle, |\downarrow\rangle, |0\rangle\}$. This base must be rewritten according to the symmetry quantum number to coupled it with the matrices at the NRG code.

- **DM-NRG**: As described in subsection 3.2.5, this code generates iteratively the density matrix associated to each energy scale. Then it computes the green function and the density of states. The DOS of the single *QD* model is an example of its outputs. The plot shows the characteristic Kondo peak at the Fermi energy in the middle of the Coulomb peaks describing the energy states.

This NRG code was previously implemented in C++. It can be cloned from the Github link `https://git.io/fh9cM`. To optimize the performance of NRG, the code uses the packages Boost, LAPACK and Gnu Scientific Library (GSL), which provide a rapid interface for numerical matrix diagonalization.

3.2.7 NRG for a double quantum dot

In this subsection we will observe the results of the NRG code applied to a double quantum dot attached to a metalic lead. The initial Hamiltonian for this system has initial dimension of 16. While the symmetries in this Hamiltonian are exactly the same than the ones in the single QD case $\mathscr{N}S$. However, we decided to use another symmetry to solve this system. This system was simulated using the code for a DQD-Majorana coupling presented on **??** by setting the Majorana couplings to $t_1 = t_2 = 0$. The viability of these result and its correspondence with previous works is an important test that supports our results.

We ran the NRG code for the DQD with the coulomb repulsion parameter equal to

$$U_1 = U_2 = 17.7305. \tag{3.43}$$

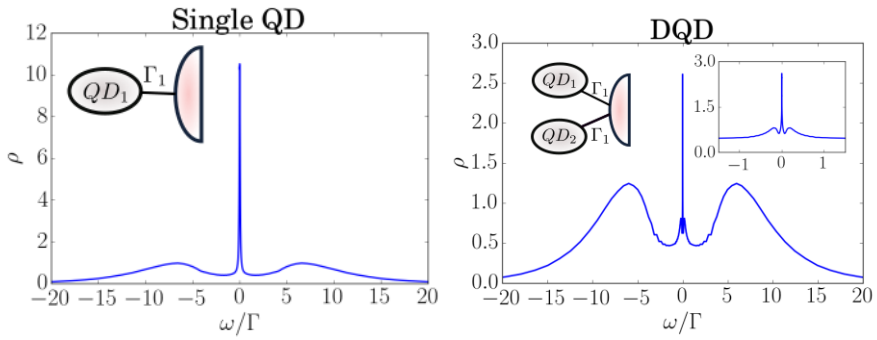

(a) (b) $\Gamma_2 = \Gamma_1$. Inset: Low energy DOS.

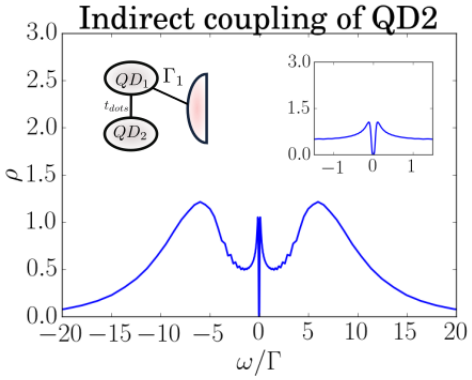

(c) $t_{dots} = 0.689\Gamma$. Low energy DOS.

Figure 3.8: Density of states in QD1 predicted by NRG at each case. The insets show the. Note that figure a) is in a different scale due to a major central peak ..

Source: *By the Author*

We used the same configurations from Figure 3.2.

The single QD attached to a metallic lead is a particular case of the double quantum dot model, where the second dot is not attached $\Gamma_2 = t_{dots} = 0$. Figure 3.8 shows the NRG results for this case. The three plots show the external Coulomb peaks at $e_1 = \frac{U}{2} \sim 8.62\Gamma_1$, which represent the DOS of the energy levels. In addition Figure 3.8a shows a central peak at the Fermi energy. **This is the Kondo Peak**.

In Figure 3.8b we observe the DOS when the two QDs are symmetrically attached. At low energies, the inset shows the appearance of two satellite peaks representing the Ruderman-Kittel-Kasuya-Yosida (RKKY) interaction. This is an anti-ferromagnetic coupling that appears in the interacting case due to the strong correlations between both dots. A detailed explanation of the appearance of these new states is included in section Appendix B.

The most interesting case is in Figure 3.8c. As we already observed in the non-interacting

case, the interference with the second dot completely destroys the Kondo peak. This effect is observed at low energies closed to $t_{dots} = 0.689\Gamma$. The paper describing this result was a central part of one of my advisor's project. This result encouraged me to formulate the following question. What happens if we attached a Majorana mode to one of these dots?. Would it e destroyed by interference or it will survive to it. Answering this question is one of the mean objectives of chapter **??**.

Bibliography

[1] A. Yu Kitaev. Unpaired Majorana fermions in quantum wires. *Phys.-Usp.*, 44(10S):131, 2001. ISSN 1063-7869. doi: 10.1070/1063-7869/44/10S/S29. URL http://stacks.iop.org/1063-7869/44/i=10S/a=S29. 1

[2] Jason Alicea. Majorana fermions in a tunable semiconductor device. *Phys. Rev. B*, 81 (12):125318, March 2010. doi: 10.1103/PhysRevB.81.125318. URL https://link.aps.org/doi/10.1103/PhysRevB.81.125318. 1

[3] Jason Alicea. New directions in the pursuit of Majorana fermions in solid state systems. *Rep. Prog. Phys.*, 75(7):076501, 2012. ISSN 0034-4885. doi: 10.1088/0034-4885/75/7/076501. URL http://stacks.iop.org/0034-4885/75/i=7/a=076501. 1

[4] Dong E. Liu and Harold U. Baranger. Detecting a majorana-fermion zero mode using a quantum dot. 84(20). ISSN 1098-0121, 1550-235X. doi: 10.1103/PhysRevB.84.201308. URL http://arxiv.org/abs/1107.4338. 1

[5] Minchul Lee, Jong Soo Lim, and Rosa Lopez. Kondo effect in a quantum dot side-coupled to a topological superconductor. 87(24):241402. doi: 10.1103/PhysRevB.87.241402. URL https://link.aps.org/doi/10.1103/PhysRevB.87.241402. 1

[6] E. Vernek, P. H. Penteado, A. C. Seridonio, and J. C. Egues. Subtle leakage of a majorana mode into a quantum dot. 89(16):165314. doi: 10.1103/PhysRevB.89.165314. URL https://link.aps.org/doi/10.1103/PhysRevB.89.165314. 1

[7] M. T. Deng, S. Vaitiekenas, E. B. Hansen, J. Danon, M. Leijnse, K. Flensberg, J. Nygard, P. Krogstrup, and C. M. Marcus. Majorana bound state in a coupled quantum-dot hybrid-nanowire system. 354(6319):1557–1562. ISSN 0036-8075, 1095-9203. doi: 10.1126/science.aaf3961. URL http://science.sciencemag.org/content/354/6319/1557. 1

[8] David A. Ruiz-Tijerina, E. Vernek, Luis G. G. V. Dias da Silva, and J. C. Egues. Interaction effects on a majorana zero mode leaking into a quantum dot. 91(11):115435. doi: 10.1103/PhysRevB.91.115435. URL https://link.aps.org/doi/10.1103/PhysRevB.91.115435. 1

[9] Daniel A Spielman. Algorithms, graph theory, and linear equations in laplacian matrices. In *Proceedings of the International Congress of Mathematicians*, volume 4, pages 2698–2722, 2010. URL http://www.mathunion.org/ICM/ICM2010.4/Main/icm2010.4.2698.2722.pdf. 3.1.1, 3.1.1

[10] Ralf Bulla, Theo A. Costi, and Thomas Pruschke. Numerical renormalization group method for quantum impurity systems. *Reviews of Modern Physics*, 80(2):395–450, April 2008. doi: 10.1103/RevModPhys.80.395. URL https://link.aps.org/doi/10.1103/RevModPhys.80.395. 3.2.1, 3.2.1, A.1

[11] Kenneth G. Wilson. The renormalization group: Critical phenomena and the Kondo problem. *Reviews of Modern Physics*, 47(4):773–840, October 1975. doi: 10.1103/RevModPhys.47.773. URL https://link.aps.org/doi/10.1103/RevModPhys.47.773. 3.2.1

[12] H. R. Krishna-murthy, J. W. Wilkins, and K. G. Wilson. Renormalization-group approach to the Anderson model of dilute magnetic alloys. 1. Static properties for the symmetric case. *Phys.Rev.*, B21:1003–1043, 1980. doi: 10.1103/PhysRevB.21.1003. 3.2.1, 3.2.1, A.1, A.1

[13] T. A. Costi, A. C. Hewson, and V. Zlatic. Transport coefficients of the Anderson model via the numerical renormalization group. *Journal of Physics: Condensed Matter*, 6(13):2519, 1994. ISSN 0953-8984. doi: 10.1088/0953-8984/6/13/013. URL http://stacks.iop.org/0953-8984/6/i=13/a=013. 3.2.5

[14] Walter Hofstetter. Generalized Numerical Renormalization Group for Dynamical Quantities. *Physical Review Letters*, 85(7):1508–1511, August 2000. doi: 10.1103/PhysRevLett.85.1508. URL https://link.aps.org/doi/10.1103/PhysRevLett.85.1508. 3.2.5

[15] Wanda C. Oliveira and Luiz N. Oliveira. Generalized numerical renormalization-group method to calculate the thermodynamical properties of impurities in metals. *Physical Review B*, 49(17):11986–11994, May 1994. doi: 10.1103/PhysRevB.49.11986. URL https://link.aps.org/doi/10.1103/PhysRevB.49.11986. 3.2.6

[16] Michael Sindel. *Numerical Renormalization Group studies of Quantum Impurity Models in the Strong Coupling Limit*. Text.PhDThesis, Ludwig-Maximilians-UniversitÃt MÃŒnchen, January 2005. URL https://edoc.ub.uni-muenchen.de/3115/. A.1

[17] M. A. Ruderman and C. Kittel. Indirect Exchange Coupling of Nuclear Magnetic Moments by Conduction Electrons. *Physical Review*, 96(1):99–102, October 1954. doi: 10.1103/PhysRev.96.99. URL https://link.aps.org/doi/10.1103/PhysRev.96.99.B

[18] Kei Yosida. Magnetic Properties of Cu-Mn Alloys. *Physical Review*, 106(5):893–898, June 1957. doi: 10.1103/PhysRev.106.893. URL https://link.aps.org/doi/10.1103/PhysRev.106.893. B

Appendix A

Appendix

A.1 From the logarithmic discretization to the Wilson's chain.

Logarithmic Discretization:

We start with an Anderson model Hamiltonian such as the one in (**??**) without magnetic field

$$H = \frac{U}{2} + \sum_{\sigma}\left[\left(\varepsilon_d + \frac{U}{2}\right) d_\sigma^\dagger d_\sigma + \frac{U}{2}(d_\sigma^\dagger d_\sigma - 1)^2 + \sum_{\mathbf{k}} \varepsilon_{\mathbf{k}} c_{\mathbf{k}\sigma}^\dagger c_{\mathbf{k}\sigma} + V_{\mathbf{k}} d_\sigma^\dagger c_{\mathbf{k}\sigma} + V_{\mathbf{k}}^* c_{\mathbf{k}\sigma}^\dagger d_\sigma\right]. \tag{A.1}$$

At low-energies we can assume that QD couples only to s-wave states in the leads[12]. This implies that that the Fermi surface is contained in a single, isotropic conduction band extending inside some fixed cutoffs $-D$ and D. Thus, $\varepsilon_{\mathbf{k}}$ only depends on $|\mathbf{k}|$. This makes possible to transform the sum over $\mathbf{k}$ in equation A.1 into an integral over ε between the energy cutoffs

$$\begin{aligned} H \quad = \sum_\sigma \quad & \left[\left(\varepsilon_d + \frac{U}{2}\right) d_\sigma^\dagger d_\sigma + \frac{U}{2}(d_\sigma^\dagger d_\sigma - 1)^2 + \int_{-D}^{D} \mathrm{d}\varepsilon\ \varepsilon c_{\varepsilon\sigma}^\dagger c_{\varepsilon\sigma} \right. \\ & \left. + \int_{-D}^{D} \sqrt{\rho_\sigma(\varepsilon)}\mathrm{d}\varepsilon\ V_\varepsilon d_\sigma^\dagger c_{\mathbf{k}\sigma} + V_\varepsilon^* c_{\varepsilon\sigma}^\dagger d_\sigma\right]. \end{aligned} \tag{A.2}$$

Here $c_{\varepsilon\sigma}^\dagger$ creates an electron with energy ε and $\rho_\sigma(\varepsilon)$ is the density of states of the system per spin, which appears in the integral due to the change of variable from $\mathbf{k}$ to $\varepsilon \propto |\mathbf{k}|^2$. Finally, we ignore the energy dependence of ρ and V_d and we replace them by their values in the Fermi energy (This approximation has no great relevance which is justified in [12]) and we renormalize the energy band doing the replacements $k = \frac{\varepsilon}{D}$ and $c_{k\sigma} := \sqrt{D} c_{\varepsilon\sigma}$ so that (A.2) becomes

$$H = D\sum_{\sigma}\left[\frac{1}{D}\left(\varepsilon_d+\frac{U}{2}\right)d^{\dagger}_{\sigma}d_{\sigma}+\frac{U}{2D}(d^{\dagger}_{\sigma}d_{\sigma}-1)^2+\int_{-1}^{1}\mathrm{d}k\; kc^{\dagger}_{k\sigma}c_{k\sigma}\right.$$
$$\left.+\sqrt{\frac{\Gamma}{\pi D}}\int_{-1}^{1}\mathrm{d}k\; d^{\dagger}_{\sigma}c_{k\sigma}+c^{\dagger}_{k\sigma}d_{\sigma}\right] \tag{A.3}$$
$$= H_d+D\sum_{\sigma}\left[\int_{-1}^{1}\mathrm{d}k\; kc^{\dagger}_{k\sigma}c_{k\sigma}+\sqrt{\frac{\Gamma}{\pi D}}\int_{-1}^{1}\mathrm{d}k\; d^{\dagger}_{\sigma}c_{k\sigma}+c^{\dagger}_{k\sigma}d_{\sigma}\right], \tag{A.4}$$

where $\Gamma=\pi\rho V^2$ is associated to the lever-width [16, (3.5)]. At this point we have our model dependent of three unit-less constants $\frac{\varepsilon_d}{D}$, $\frac{U}{2D}$ and $\frac{\Gamma}{\pi D}$. The logarithmic discretization starts by defining an scaling parameter $\Lambda\geq 1$ in diving the energy domain $[-1,1]$ into an array of intervals of the form $\{[\pm\Lambda^{-(n+1)},\pm\Lambda^{n}]\}_{n\in\mathbb{N}}$, as we can observe in **??**. Note that the width of these intervals is decreasing exponentially by

$$d_n=\Lambda^{-n}\left(1-\Lambda^{-1}\right).$$

Then inside of these energy intervals we can define a set of orthonormal Fourier series of the form

$$\phi^{\pm}_{np}(\varepsilon)=\begin{cases}\frac{1}{\sqrt{d_n}}e^{\pm i\omega_n p\varepsilon} & \varepsilon\in[\pm\Lambda^{-(n+1)},\pm\Lambda^{n}]\\ 0 & \text{a.o.c}\ ,\end{cases} \tag{A.5}$$

with $\omega_n:=\frac{2\pi}{d_n}$ so that $\phi^{\pm}_{np}\left(\pm\Lambda^{-(n+1)}\right)=\phi^{\pm}_{np}\left(\pm\Lambda^{-n)}\right)$. Then we can decompose the creation operators $c^{\dagger}_{k}$ into their interval-Fourier contributions as

$$c^{\dagger}_{k\sigma}=\sum_{np}\phi^{+}_{np}(k)c^{+\dagger}_{np\sigma}+\phi^{-}_{np}(k)c^{-\dagger}_{np\sigma} \tag{A.6}$$

with the new creation operators defined as

$$c^{\pm\dagger}_{np\sigma}:=\left(c^{\pm}_{np\sigma}\right)^{\dagger}=\int_{-1}^{1}\mathrm{d}\varepsilon\;\left[\phi^{+}_{np}(\varepsilon)\right]^{*}c^{\dagger}_{\varepsilon\sigma}.$$

This decomposition (A.6) is a simple consequence of the orthonormality of the functions defined in (A.5). In addition we can readily proof that $c^{\pm\dagger}_{np\sigma}$-operators satisfy the anti-commutation relations, so that they are rightful fermionic creation operators.

We can now use (A.6) to replace the k-dependent terms in hamiltonian (A.3). Then we obtain

$$\begin{aligned}
\int_{-1}^{1} \mathrm{d}k\, c^{\dagger}_{k\sigma} d_{\sigma} &= \int_{-1}^{1} \mathrm{d}k \left(\sum_{np} \phi^{+}_{np}(k) c^{+\dagger}_{np\sigma} + \phi^{-}_{np}(k) c^{-\dagger}_{np\sigma} \right) d_{\sigma} \\
&= \left(\sum_{np} \left(\int_{-1}^{1} \mathrm{d}k\, \phi^{+}_{np}(k) \right) c^{+\dagger}_{np\sigma} + \left(\int_{-1}^{1} \mathrm{d}k\, \phi^{-}_{np}(k) \right) c^{-\dagger}_{np\sigma} \right) d_{\sigma} \\
&= \left(\sum_{np} \left(\int_{\Lambda^{-(n+1)}}^{\Lambda^{-n}} \mathrm{d}k\, \frac{e^{i\omega_n pk}}{\sqrt{d_n}} \right) c^{+\dagger}_{np\sigma} + \left(\int_{-\Lambda^{-n}}^{-\Lambda^{-(n+1)}} \mathrm{d}k\, \frac{e^{-i\omega_n pk}}{\sqrt{d_n}} \right) c^{-\dagger}_{np\sigma} \right) d_{\sigma} \\
&= \left(\sum_{np} \sqrt{d_n} \delta_p c^{+\dagger}_{np\sigma} + \sqrt{d_n} \delta_p c^{-\dagger}_{np\sigma} \right) d_{\sigma} \\
&= \sqrt{1-\Lambda^{-1}} \sum_{n} \Lambda^{-\frac{n}{2}} \left(c^{+\dagger}_{np\sigma} + c^{-\dagger}_{np\sigma} \right) d_{\sigma}. \qquad \text{(A.7)}
\end{aligned}$$

And

$$\begin{aligned}
\int_{-1}^{1} \mathrm{d}k\, k c^{\dagger}_{k\sigma} c_{k\sigma} &= \sum_{n,n',p,p'} \sum_{s,s'=\pm} \left(\int_{-1}^{1} k \mathrm{d}k\, \phi^{s}_{np}(k) \left(\phi^{s'}_{np}(k) \right)^{*} \right) c^{s\dagger}_{np\sigma} c^{s'}_{n'p'\sigma} \\
&= \sum_{n,n',p,p'} \sum_{s,s'=\pm} \left(\frac{\delta_{nn'}\delta_{ss'}}{d_n} \int_{\Lambda^{-(n+1)}}^{\Lambda^{-n}} k \mathrm{d}k\, e^{is\omega_n k(p-p')} \right) c^{s\dagger}_{np\sigma} c^{s}_{np'\sigma} \\
&= \sum_{npp'} \sum_{s=\pm} \left(\frac{s}{2} \Lambda^{-2n} \left(1-\Lambda^{-2} \right) \delta_{pp'} + \frac{1-\delta_{pp'}}{is\omega_n (p-p')} \left[k e^{is\omega_n k(p-p')} \right]_{\Lambda^{-(n+1)}}^{\Lambda^{-n}} \right) \frac{c^{s\dagger}_{np\sigma} c^{s'}_{np'\sigma}}{d_n} \\
&= \frac{1}{2} \left(1+\Lambda^{-1} \right) \sum_{np} \Lambda^{-n} \left(c^{+\dagger}_{np\sigma} c^{+}_{np\sigma} - c^{-\dagger}_{np\sigma} c^{-}_{np\sigma} \right) \\
&\qquad + \sum_{n} \sum_{p \neq p'} \frac{1-\Lambda^{-1}}{2i\pi (p'-p)} \left(c^{+\dagger}_{np\sigma} c^{+}_{np'\sigma} - c^{-\dagger}_{np'\sigma} c^{-}_{np\sigma} \right) e^{\frac{2i\pi(p-p')}{1-\Lambda^{-1}}}. \qquad \text{(A.8)}
\end{aligned}$$

Thus, if we replace (A.7) and (A.8) into (A.3) we will obtain a logarithmic discretization of the hamiltonian. The next part will we to map this discretization to an iterative process that is worth for a numerical computations.

Mapping the Anderson model to a Chain-Hamiltonian

We are looking for a model just like the one we have in the right part of Figure 3.3. This is because a Chain-Hamiltonian will give an iterative approximation of the Anderson model with an increasing (but still controllable) number of degrees of freedom. This will provide the rightful structure for a numerical diagonalization of the hamiltonian.

To do this, observe from equations (A.7),(A.8) that the QD (d_σ) couples directly only to the operators with $p=0\left(c^{\pm\dagger}_{n0\sigma}\right)$. The $p\neq 0$ terms will appear in the hamiltonian only because they are coupled to $c^{+\dagger}_{np\sigma}$ in Equation (A.8). Thus, as a first approximation we can neglect all terms in (A.8) with $p\neq 0$. This leaves only the first part of (A.8), so that we can define $c^{\pm\dagger}_{n\sigma}:=c^{\pm\dagger}_{np\sigma}$. Let

$$f^\dagger_{0\sigma}=\sqrt{\frac{1-\Lambda^{-1}}{2}}\sum_n \Lambda^{-\frac{n}{2}}\left(c^{+\dagger}_{n\sigma}+c^{-\dagger}_{n\sigma}\right),\ \text{so that}\ \sqrt{2}f^\dagger_{0\sigma}d_\sigma=\int_{-1}^{1}\mathrm{d}k\ c^\dagger_{k\sigma}d_\sigma. \tag{A.9}$$

Note $\left\{f^\dagger_{0\sigma},f_{0\sigma}\right\}=\frac{1-\Lambda^{-1}}{2}\sum_n 2\Lambda^{-n}=1$. Replacing this in (A.3)we get

$$H=H_d+D\sum_\sigma\left[\sqrt{\frac{2\Gamma}{\pi D}}\left(d^\dagger_\sigma f_{0\sigma}+f^\dagger_{0\sigma}d_\sigma\right)+\frac{1}{2}\left(1+\Lambda^{-1}\right)\sum_n\Lambda^{-n}\left(c^{+\dagger}_{n\sigma}c^{+}_{n\sigma}-c^{-\dagger}_{n\sigma}c^{-}_{n\sigma}\right)\right].$$

$f^\dagger_0$will represent the first site of the chain-hamiltonian in **??** since no other term is coupled to the dot hamiltonian. We also have the coupling term $\xi_0=\sqrt{\frac{2\Gamma}{\pi D}}$. It is possible to obtain the following $f^\dagger_m$-operators by supposing a solution of the form

$$f^\dagger_{m\sigma}=\sum_n a^+_{mn}c^{+\dagger}_{n\sigma}+a^-_{mn}c^{-\dagger}_{n\sigma}=\sum_n\sum_{s=\pm}a^s_{mn}c^{s\dagger}_{n\sigma}, \tag{A.10}$$

such that they satisfy the anti-commutation relations

$$\left\{f^\dagger_{m\sigma},f_{m\sigma}\right\}=\delta_{mm'}\delta_{\sigma\sigma'}\ ,\ \left\{f^\dagger_{m\sigma},f^\dagger_{m\sigma}\right\}=\left\{f^\dagger_{m\sigma},f^\dagger_{m\sigma}\right\}=0$$

and

$$\frac{1}{2}\left(1+\Lambda^{-1}\right)\sum_n\Lambda^{-n}\left(c^{+\dagger}_{n\sigma}c^{+}_{n\sigma}-c^{-\dagger}_{n\sigma}c^{-}_{n\sigma}\right)=\sum_{m=0}^{\infty}\Lambda^{\frac{-m}{2}}\xi_m\left(f^\dagger_{m\sigma}f_{m+1,\sigma}+f^\dagger_{m+1\sigma}f_{m\sigma}\right). \tag{A.11}$$

It is possible to find a solution for this system using the formula of the right part of equation A.11. Since the relation is only given between consecutive terms $m,m+1$ and we already have the coefficients for $m=0$ $\left(a^s_{0n}=\sqrt{\frac{1-\Lambda^{-1}}{2}}\Lambda^{-\frac{n}{2}}\right)$. Then it is possible to determine the upper coefficients in a recursive way starting from $m=0$. Supposing we can obtain the m^{th}-coefficients (a^s_{mn}) and then finding iteratively the coefficients of $m+1$ (a^s_{mn}) using the relation given by equation (A.11). This provides a numerical way for obtaining the $f^\dagger_{m\sigma}$ operators. In fact in our case, where we actually did important assumptions, the problem can be solved analytically obtaining that the final Hamiltonian is given by

$$H=H_d+D\sum_\sigma\left[\sqrt{\frac{2\Gamma}{\pi D}}\left(d^\dagger_\sigma f_{0\sigma}+f^\dagger_{0\sigma}d_\sigma\right)+\frac{1}{2}\left(1+\Lambda^{-1}\right)\sum_{n=0}^{\infty}\Lambda^{\frac{-n}{2}}\xi_n\left(f^\dagger_{n\sigma}f_{n+1,\sigma}+f^\dagger_{n+1\sigma}f_{n\sigma}\right)\right]. \tag{A.12}$$

with

$$\xi_n = \frac{1-\Lambda^{-n-1}}{\left(1-\Lambda^{-2n-1}\right)^{\frac{1}{2}}\left(1-\Lambda^{-2n-3}\right)^{\frac{1}{2}}}.$$

The formal recursive-solution of this problem can be found in [10] . Note that equation (A.12) describes the chain hamiltonian model that we where looking for in **??**. Note that in the limit when $n \longrightarrow \infty$

$$\Lambda^{\frac{-n}{2}}\xi_n \longrightarrow \frac{\Lambda^{\frac{-n}{2}}\left(1-\Lambda^{-n}\right)}{1-\Lambda^{-2n}} \sim \frac{\Lambda^{\frac{-n}{2}}}{1+\Lambda^{-n}},$$

which implies an exponential decaying of the hopping term in the chain.

Appendix B

Three peak appearance in the Double Quantum Dot model.

The DQD model is characterized by the formation of a new state that entangles the two Quantum dots through the leads. This produces an anti-ferromagnetic interaction between the QDs, commonly known as Ruderman-Kittel-Kasuya-Yosida (RKKY) interaction [17, 18]. As consequense, two satelite peaks will emerge in the Density of States.

To explain this phenomenon we will take a symmetric version of Hamiltonian (**??**) with $2e_i = U_i = U$, $t_i = t$ and $t_{dots} = 0$ for $i \in \{1,2\}$.

$$H = \sum_{i,k,\sigma} \frac{U_i}{2}(d^\dagger_{i\sigma}d_{i\sigma} - 1)^2 + t(d_{+,\downarrow} + d^\dagger_{+,\downarrow})\gamma_1 + \Gamma_i(d^\dagger_{i\sigma}c_{k\sigma} + c^\dagger_{k\sigma}d_{i\sigma}). \tag{B.1}$$

The symmetry of the previous Hamiltonian is suitable to apply a base change of the form

$$d_{+,\sigma} = \frac{1}{\sqrt{2}}(d_{1\sigma} + d_{2\sigma}) \ , \ d_{-,\sigma} = \frac{1}{\sqrt{2}}(d_{1\sigma} - d_{2\sigma}).$$

These new operators satisfy the fermionic anti-commutation relations

$$\{d_{\pm,\sigma}, d^\dagger_{\pm,\sigma}\} = 1, \{d_{\pm,\sigma}, d^\dagger_{\mp,\sigma}\} = 0,$$

so that the may be considered as fermion operators. All lineal terms in (B.1) are trivially adapted to the new base. The repulsion potential

$$\sum_i (\sum_\sigma d^\dagger_{i\sigma}d_{i\sigma} - 1)^2 = (\sum_\sigma d^\dagger_{1\sigma}d_{1\sigma} - 1)^2 + (\sum_\sigma d^\dagger_{2\sigma}d_{2\sigma} - 1)^2.$$

gives rise to a non-trivial interaction between the new states. To find this interaction we define the particle number operator

$$\hat{n}_{i,\sigma} := d^\dagger_{i,\sigma}d_{i,\sigma}.$$

So that

$$\hat{n}_{1,\sigma} = \frac{1}{2}\left(\hat{n}_{+,\sigma} + \hat{n}_{-,\sigma} + d^\dagger_{+,\sigma}d_{-,\sigma} + d^\dagger_{-,\sigma}d_{+,\sigma}\right) = \frac{1}{2}\left(\hat{N}_\sigma + \hat{E}_\sigma\right),$$

with $\hat{N} = \hat{n}_{+,\sigma} + \hat{n}_{-,\sigma}$ and $\hat{E}_\sigma = d^\dagger_{+,\sigma}d_{-,\sigma} + d^\dagger_{-,\sigma}d_{+,\sigma}$. Similarly

$$\hat{n}_{2,\sigma} = \frac{1}{2}\left(\hat{N}_\sigma - \hat{E}_\sigma\right).$$

Hence

$$\sum_i (\sum_\sigma d^\dagger_{i\sigma} d_{i\sigma} - 1)^2 = \left(\frac{\hat{N}+\hat{E}}{2} - 1\right)^2 + \left(\frac{\hat{N}-\hat{E}}{2} - 1\right)^2 = \frac{\left(\hat{N}-2\right)^2 - \hat{E}^2}{2},$$

with $\hat{N} = \sum_\sigma \hat{N}_\sigma$, $\hat{E} = \sum_\sigma \hat{E}_\sigma$. Note that opeator $\hat{N}$ represents the total occupation number inside both dots. If this occupation is different than 2 there is an imbalance between particles and dots that is punished by this term. The term E^2 is much more interesting since this one is the responsible for the emergence of satellite peaks in the DOS. To understand what it makes it is simple to observe its results when applied to a based ordered by $|+,-\rangle$.

$$\hat{E}^2|\uparrow,0\rangle = \hat{E}|0,\uparrow\rangle = |\uparrow,0\rangle$$

$$\hat{E}^2|\uparrow,\downarrow\rangle = \hat{E}\left(|0,\uparrow\downarrow\rangle + |\uparrow\downarrow,0\rangle\right) = 2|\uparrow,\downarrow\rangle - 2|\downarrow,\uparrow\rangle$$

The new Hamiltonian

$$H = \sum_\sigma \frac{U}{4}\left(\left(\hat{N}-2\right)^2 - \hat{E}^2\right) + \frac{t}{\sqrt{2}}(d_{+,\downarrow} + d^\dagger_{+,\downarrow})\gamma_1 + \frac{\Gamma}{\sqrt{2}}\sum_k (d^\dagger_{+,\sigma} c_{k\sigma} + c^\dagger_{k\sigma} d_{+,\sigma}) \tag{B.2}$$

is represented in **??**

We can explain this three-peak as the result of a new strong coupling interaction characterized by the spin exchange between both dots.

In addition, the spin-up DOS at the Fermi energy grows faster than the spin-down DOS, breaking the initial spin-symmetry when $t_1 = t_2 = 0$. At $t_1 = t_2 = 0.02D$ the spin-up DOS at the fermi energy doubles the spin-down DOS which implies that the Majorana signature is present in both dots. Indeed **??** shows that the relation $\frac{\rho_\uparrow(0)}{\rho_\uparrow(0)}$ increases continuously from 1 to 2. Note that the Majorana is completely attached when the coupling t_1 reaches the order of $0.01D$.

B.1 Initial DQD-Majorana Hamiltonian.

$H_{N_\uparrow=0,P_\downarrow=-1}$:

$$\begin{array}{c} |\downarrow,\downarrow,\downarrow\rangle \rightarrow \\ |0,0,\downarrow\rangle \rightarrow \\ |0,\downarrow,0\rangle \rightarrow \\ |\downarrow,0,0\rangle \rightarrow \end{array} \begin{bmatrix} \varepsilon_d^+ + \frac{U^+}{2} - 2h + \varepsilon_m & 0 & -\tilde{t}_{+1} & \tilde{t}_{+2} \\ 0 & \frac{U^+}{2} + \varepsilon_m & \tilde{t}^*_{-2} & \tilde{t}^*_{-1} \\ -\tilde{t}^*_{+1} & \tilde{t}_{-2} & \varepsilon_{d_2} + \frac{U^+}{2} - h - \varepsilon_m & t \\ \tilde{t}^*_{+2} & \tilde{t}_{-1} & t^* & \varepsilon_{d_1} + \frac{U^+}{2} - h - \varepsilon_m \end{bmatrix}$$

$H_{N_\uparrow=0,P_\downarrow=1}$:

$$\begin{array}{c} |0,0,0\rangle \to \\ |\downarrow,\downarrow,0\rangle \to \\ |\downarrow,0,\downarrow\rangle \to \\ |0,\downarrow,\downarrow\rangle \to \end{array} \begin{bmatrix} \frac{U^+}{2}-\varepsilon_m & 0 & \tilde{t}_{+1} & \tilde{t}_{+2} \\ 0 & \varepsilon_d^+ + \frac{U^+}{2} - 2h - \varepsilon_m & \tilde{t}^*_{-2} & -\tilde{t}^*_{-1} \\ \tilde{t}^*_{+1} & \tilde{t}_{-2} & \varepsilon_{d_1} + \frac{U^+}{2} - h + \varepsilon_m & t \\ \tilde{t}^*_{+2} & -\tilde{t}_{-1} & t^* & \varepsilon_{d_2} + \frac{U^+}{2} - h + \varepsilon_m \end{bmatrix}$$

$H_{N_\uparrow=2,P_\downarrow=-1}$:

$$\begin{array}{c} |\uparrow\downarrow,\uparrow\downarrow,\downarrow\rangle \to \\ |\uparrow,\uparrow,\downarrow\rangle \to \\ |\uparrow,\uparrow\downarrow,0\rangle \to \\ |\uparrow\downarrow,\uparrow,0\rangle \to \end{array} \begin{bmatrix} 2\varepsilon_d^+ + \frac{3U^+}{2} + \varepsilon_m & 0 & \tilde{t}_{+1} & \tilde{t}_{+2} \\ 0 & \varepsilon_d^+ + \frac{U^+}{2} + 2h + \varepsilon_m & \tilde{t}^*_{-2} & -\tilde{t}^*_{-1} \\ \tilde{t}^*_{+1} & \tilde{t}_{-2} & f(d_1,d_2) + h - \varepsilon_m & -t \\ \tilde{t}^*_{+2} & -\tilde{t}_{-1} & -t^* & f(d_2,d_1) + h - \varepsilon_m \end{bmatrix}$$

with $f(d_i,d_j) = \varepsilon_{d_i} + \frac{U_i}{2} + 2\varepsilon_{d_j} + \frac{3U_j}{2}$.

$H_{N_\uparrow=2,P_\downarrow=1}$:

$$\begin{array}{c} |\uparrow,\uparrow,0\rangle \to \\ |\uparrow\downarrow,\uparrow\downarrow,0\rangle \to \\ |\uparrow\downarrow,\uparrow,\downarrow\rangle \to \\ |\uparrow,\uparrow\downarrow,\downarrow\rangle \to \end{array} \begin{bmatrix} \varepsilon_d^+ + \frac{U^+}{2} + 2h - \varepsilon_m & 0 & -\tilde{t}_{+1} & \tilde{t}_{+2} \\ 0 & 2\varepsilon_d^+ + \frac{3U^+}{2} - \varepsilon_m & \tilde{t}^*_{-2} & \tilde{t}^*_{-1} \\ -\tilde{t}^*_{+1} & \tilde{t}_{-2} & f(d_2,d_1) + h + \varepsilon_m & -t \\ \tilde{t}^*_{+2} & \tilde{t}_{-1} & -t^* & f(d_1,d_2) + h + \varepsilon_m \end{bmatrix}$$